Atomic long-range order effects on Curie temperature and adiabatic spin-wave dynamics in strained Fe-Co alloy films

Stephan Schönecker,[1,*] Xiaoqing Li,[1,2,†] Börje Johansson,[1,2] and Levente Vitos[1,2,3]

[1]*Applied Materials Physics, Department of Materials Science and Engineering, KTH-Royal Institute of Technology, Stockholm SE-10044, Sweden*

[2]*Department of Physics and Astronomy, Division of Materials Theory, Uppsala University, Box 516, SE-75120, Uppsala, Sweden*

[3]*Research Institute for Solid State Physics and Optics, Wigner Research Center for Physics, Budapest H-1525, P.O. Box 49, Hungary*

(Received 2 May 2016; revised manuscript received 9 July 2016; published 9 August 2016)

The strained Fe-Co alloy in body-centered tetragonal (bct) structure has raised considerable interest due to its giant uniaxial magnetocrystalline anisotropy energy. On the basis of the classical Heisenberg Hamiltonian with *ab initio* interatomic exchange interactions, we perform a theoretical study of fundamental finite temperature magnetic properties of $Fe_{1-x}Co_x$ alloy films as a function of three variables: chemical composition $0.3 \leqslant x \leqslant 0.8$, bct geometry $[a,c(a)]$ arising from in-plane strain and associated out-of-plane relaxation, and atomic long-range order (ALRO). The Curie temperatures $T_C(x,a)$ obtained from Monte Carlo simulations display a competition between a pronounced dependence on tetragonality, strong ferromagnetism in the Co-rich alloy, and the beginning instability of ferromagnetic order in the Fe-rich alloy when $c/a \to \sqrt{2}$. Atomic ordering enhances T_C and arises mainly due to different distributions of atoms in neighboring coordination shells rather than altering exchange interactions significantly. We investigate the ordering effect on the shape of the adiabatic spin-wave spectrum for selected pairs (x,a). Our results indicate that long-wavelength acoustic spin-wave excitations show dependencies on x, a, and ALRO similar to those of T_C. The directional anisotropy of the spin-wave stiffness $d(x,a)$ peaks in narrow ranges of composition and tetragonality. ALRO exhibits a strong effect on d for near equiconcentration Fe-Co. We also discuss our findings in the context of employing Fe-Co as perpendicular magnetic recording medium.

DOI: 10.1103/PhysRevB.94.064410

I. INTRODUCTION

The magnetic properties of the Fe-Co binary alloy have attracted researchers for a long time. The ferromagnetic Fe-Co phase in the body-centered cubic (bcc) structure is well known to maximize the concentration-dependent mean atomic moment among transition-metal phases (Slater-Pauling curve) [1]. A few years ago, theory predicted a giant uniaxial magnetocrystalline anisotropy energy (MAE) in body-centered tetragonal (bct) $Fe_{1-x}Co_x$ alloy in narrow ranges of concentration x and tetragonality c/a, which, in combination with the high saturation magnetization, renders it a promising material for thin film perpendicular magnetic recording applications [2]. While the original prediction of giant MAE (Ref. [2]) was based on the virtual-crystal approximation (VCA) to treat the alloy problem, follow-up first-principles investigations showed that a more realistic treatment of chemical disorder reduces the maximum calculated uniaxial MAE in bct $Fe_{1-x}Co_x$ [3–5].

Experiments for strained Fe-Co alloy films on various fcc transition metal substrates have qualitatively confirmed large values of the MAE and verified that the appearance of a perpendicular easy axis is sensitive to both alloy composition and tetragonality [6–10]. In coherent epitaxial growth, the choice of substrates with different lattice parameters allows varying the degree of tetragonal distortion of the film in a quasicontinuous way [11,12], unless first-order lattice instabilities in the out-of-plane direction occur [13], thus enabling control of film properties.

Besides alloy composition and tetragonal distortion, it has been realized theoretically that atomic long-range order (ALRO) can have a significant effect on the MAE in bct Fe-Co [3,4]. For stoichiometric equiconcentration Fe-Co, the maximum degree of order yields the largest MAE, while imperfect long-range order was found to reduce it strongly [4]. Although a similar correlation between atomic order and magnetocrystalline anisotropy is well-known for Fe-Pt alloy [14–16], taking into account ALRO as a degree of freedom to control the magnetic properties of bct Fe-Co had not been recognized in the experiments until very recently [10].

Apart from high uniaxial MAE and saturation magnetization, suitable materials for prospective magnetic recording should also possess a Curie temperature moderately above room temperature and respond quickly to external stimulus triggering magnetization reversal, such as magnetic field or laser light [17–19]. The Curie point is particularly important in heat-assisted magnetic recording (HAMR), where locally and temporarily applied heat reduces the coercivity of the recording medium during magnetization reversal in order to comply with presently achievable write fields [18,19]. The switching speed of the magnetization vector, on the other hand, imposes physical limits on the achievable data rates and is connected to magnetization reversal and recovery processes. In field-driven magnetization reversal, in particular collective spin-wave excitations are created, which scatter in the magnetic-subsystem and decay into the thermal bath during magnetization recovery [20–22]. Thus, first-principles studies of Curie temperature and spin-wave dynamics in conjunction with understanding the details of the underlying physics

*stesch@kth.se
†xiaoqli@kth.se

are important aspects of designing materials for magnetic recording.

The aim of the present paper is, on the one hand, to characterize bct Fe-Co alloy films regarding their Curie temperature and spin-wave properties as a function of alloy composition and film geometry and, on the other hand, shed light on the impact of ALRO on both parameters. This study is mainly motivated by the aforementioned prediction that atomic order can drastically influence the MAE in this system, while such information is scarce from experiments. We show that deviations from the ordered state can significantly influence the anisotropy of the acoustic spin-wave dispersions in bct Fe-Co alloy, especially for the equiconcentration FeCo compound [23]. Our focus is on the adiabatic spin-wave dynamics with the fast spin-flip degree of freedoms decoupled from the slow motion of the spins. This approach yields a coarsened excitation spectrum and does not provide information on spin-wave lifetimes and Stoner excitations as well as their interference in contrast to more general approaches based on the transverse dynamical susceptibility [23–25] or time-dependent density-functional theory [26]. However, the adiabatic approach yields precise spin-wave dispersions and stiffness constants as well as features of long-range exchange interactions such as Kohn-anomalies [27,28].

The paper is organized as follows. In Sec. II we detail on the modeling of structure and chemical disorder in Fe-Co alloy films, introduce the magnetic model Hamiltonian used to describe the finite temperature magnetic properties, give a brief, self-contained description of how the adiabatic spin-wave dispersions and Curie temperatures were obtained, and list further computational details. In Sec. III we present and discuss results on the Curie temperature, spin-wave dispersion, and the spin-wave stiffness, alternating between homogeneously disordered alloys and inhomogeneous alloys with complete or incomplete ALRO. Section IV concludes and briefly analyzes the present findings in the context of using Fe-Co for magnetic recording applications.

II. MODELS AND COMPUTATIONAL DETAILS

A. Structure and chemical disorder

The employed structural model to describe strained tetragonal Fe-Co films follows the concept of the epitaxial Bain path (EBP) [3,29]. The EBP model assumes that interface effects on the electronic structure of the film are negligible, nonetheless the substrate-film interaction is strong enough to let the substrate dictate the in-plane lattice parameter of the film (epitaxial coherency). The achievable experimental film thicknesses are large enough to justify the bulk treatment of Fe-Co films in the context of theoretical modeling [9]. In the case of substrates with fourfold surface symmetry, e.g., the (001) facet of bcc and fcc crystals, the EBP assumes coherently grown Fe-Co films in bct geometry with in-plane film lattice parameter a (dictated by the substrate) and out-of-plane lattice parameter c. The absence of forces perpendicular to the substrate-film interface requires relaxation of c (or c/a) equivalent to minimizing the total film energy $E(a,c)$ for each a [13,30]. Notice that the experiments [6–10] realized bct Fe-Co films by means of epitaxial growth on (001) oriented

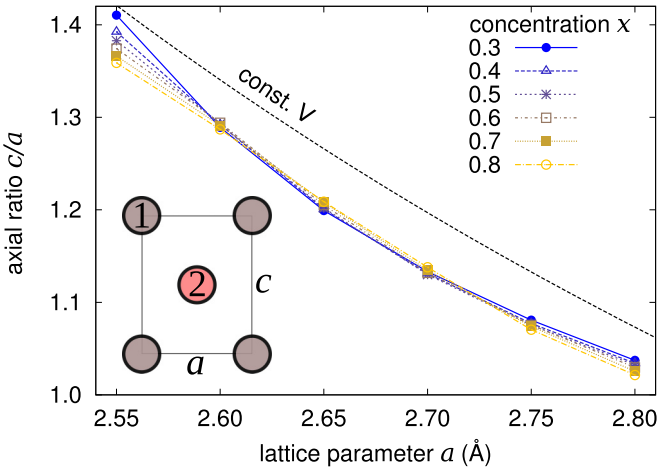

FIG. 1. Bct geometries for homogeneously random $Fe_{1-x}Co_x$ alloy obtained by relaxing the c/a ratio for each a according to the EBP model. The black dashed line (labeled "const. V") indicates the hyperbola with constant bct unit cell volume equal to the experimental volume of bcc Fe at room temperature (23.56 $Å^3$). Lines guide the eye. The inset sketches a tetragonal unit cell with concentration $Fe_{1-x+y}Co_{x-y}$ on sub-lattice "1" and $Fe_{1-x-y}Co_{x+y}$ on sublattice "2" used to model ALRO.

fcc crystals. In the following, we adopt the convention that the z axis of a Cartesian coordinate system is oriented along the tetragonal axis with fourfold rotational symmetry and that the x and y axes span the quadratic basal plane of the bct lattice.

Homogeneous chemical disorder in $Fe_{1-x}Co_x$ alloy was described by means of the coherent-potential approximation (CPA) as a basic tool of alloy theory [31]. We considered the concentration in the interval $0.3 \leqslant x \leqslant 0.8$, which approximately is the composition range where bct Fe-Co was predicted to exhibit uniaxial perpendicular magnetic anisotropy [2–4]. Chemically inhomogeneous configurations with complete or incomplete ALRO were modeled by partitioning the bct structure into two interpenetrating simple tetragonal lattices as in earlier work [4]. This approach allows for different concentrations on the sublattices and the resulting alloy state was also described by the CPA. Introducing the additional concentration variable y, the two fractional sublattice occupations are $Fe_{1-x\pm y}Co_{x\mp y}$, where the upper (lower) signs denote the composition of sub-lattice "1" ("2"); see the inset of Fig. 1 for a sketch. y is subject to the compatibility condition $0 \leqslant y \leqslant \min\{x, 1-x\}$. We notice that the case $y = 0$ corresponds to homogeneously disordered random alloys and that the ordered B2-type structure is described for $x = y = 0.5$. For $x \neq 0.5$, the upper limit on y describes the maximum B2 order compatible with the concentration x [4].

All total energy calculations were performed with the exact muffin-tin orbitals (EMTO) method [32–34] with exchange-correlation in the parametrization by Perdew, Burke, and Ernzerhof [35]. The convergence of all numerical parameters and particularly the Brillouin zone integration mesh ($27 \times 27 \times 27$ division for the total energy) was carefully checked. Magnetic order in Fe-Co was restricted to ferromagnetic states in the calculations.

B. Exchange interactions and Curie temperature

The finite temperature magnetic properties of Fe-Co were addressed through an established theoretical approach based on the adiabatic approximation for the slow spin dynamics in a fast electronic medium [36,37]. As magnetic variables of the itinerant electron system, we employ the spin-density integrated within a spherical cell around a lattice site $\boldsymbol{M}_{\mu i} = M_{\mu i}\mathbf{e}_{\mu i}$, where μ and i denote the sublattice and the unit cell, respectively. $M_{\mu i}$ is the length of the spin magnetic moment and $\mathbf{e}_{\mu i}$ its direction (normalized to unity). The underlying adiabadicity assumption is the neglect of correlations of the fast conduction-electron motion between any two lattice site magnetic moments [27,36,37].

The properties of the itinerant electron system are then mapped on a classical, nonrelativistic Heisenberg model for an alloy,

$$\mathcal{H} = -\sum_{mn}\sum_{\mu\nu}\sum_{\substack{ij\\(i\neq j \text{ if}\\ \mu=\nu)}} \chi^m_{[\mu i]}\chi^n_{[\nu j]} J^{mn}_{[\mu i][\nu j]}\mathbf{e}_{\mu i}\cdot\mathbf{e}_{\nu j}, \qquad (1)$$

where the $J^{mn}_{[\mu i][\nu j]}$ are the pair exchange interactions (the length of the magnetic moments are absorbed in the definition of J). The sums run over the alloy constituents $m,n = \{\text{Fe, Co}\}$, all sublattices μ,ν and unit cells i,j. The classical vector spin variables $\mathbf{e}_{\mu i}$ are localized at sites μi with corresponding position vectors $\boldsymbol{R}_{\mu i}$. In Eq. (1), $\chi^m_{[\mu i]}$ represents an occupation number, which equals 1 if chemical species m occupies site i on the sublattice μ and is zero otherwise [38].

The *ab initio* determination of the exchange interactions were performed in the ferromagnetic state with a standard method [39] as implemented in the EMTO-CPA method. We used a very fine k-point mesh ($43\times43\times43$ division) to ensure converged parameters for the most distant coordination shells.

The Curie temperature of the Heisenberg model Eq. (1) was obtained from classical Monte Carlo (MC) simulations with the Metropolis algorithm as implemented in the UppAsd code [40] by localizing the crossing point of the fourth-order Binder cumulant of the magnetization for different sizes of the simulation cell [41]. Fe and Co atoms were distributed on randomly selected lattice sites subject to the total alloy concentration and sublattice occupations (the atomic distribution specifies $\chi^m_{[\mu i]}$, thereby determining the corresponding set of pair interactions for a site μi). Periodic boundary conditions were employed, and the largest cell considered contained 54 000 lattice sites. All pair interactions within a shell of diameter $\approx 5a$ around a site μi were considered in the MC simulations. The spin system was equilibrated by 10 000 MC steps and measurements were performed during 50 000 steps.

For the calculation of the adiabatic spin-wave dispersions detailed in Sec. II C, we employed effective pair interactions $J_{[\mu i][\nu j]}$ defined by

$$J_{[\mu i][\nu j]} = \sum_{mn} c^m_\mu c^n_\nu J^{mn}_{[\mu i][\nu j]}, \qquad (2)$$

where, for brevity, the variable c represents the concentrations on the different sublattices for homogeneously random, partially, or fully ordered alloys. Equation (2) is the VCA average for the randomness in the exchange interactions and restores the wave vector of spin-waves as a good quantum number. Its applicability to Fe-Co was motivated by similar exchange interactions between Fe and Co [38,39]. Using the VCA average, the Heisenberg Hamiltonian Eq. (1) may be written as

$$\mathcal{H}^{\text{eff}} = -\frac{1}{N}\sum_{\mu\nu}\sum_{\substack{ij\\(i\neq j \text{ if}\\ \mu=\nu)}} J_{[\mu i][\nu j]}\mathbf{e}_{\mu i}\cdot\mathbf{e}_{\nu j}, \qquad (3)$$

with N denoting the number of unit cells. Notice that $J_{[\mu i][\nu j]}$ and $J^{mn}_{[\mu i][\nu j]}$ are identical for ordered FeCo compound.

In Sec. III C we compare adiabatic spin-wave dispersion curves obtained with the VCA average Eq. (2) to dispersion relations obtained from the dynamical structure factor $S^k(\boldsymbol{q},\omega)$ for selected cases. The latter treatment is based on spin dynamics simulations for the alloy Hamiltonian Eq. (1) performed with the UppAsd code [40] and allows addressing the effect of site disorder on spin-wave properties.

C. Adiabatic spin-wave dispersion

To Fourier transform the effective exchange interactions Eq. (2) on the underlying lattice, we employ the following index notation for position vectors and real-space exchange interactions as in earlier work [37],

$$\begin{aligned}\boldsymbol{R}_{\mu i} &= \boldsymbol{\tau}_\mu = \boldsymbol{R}_\mu, \qquad [\mu+\mathbf{0}] = \mu\\ \boldsymbol{R}_{\nu j} &= \boldsymbol{R}+\boldsymbol{\tau}_\nu = \boldsymbol{R}_{[\nu+\boldsymbol{R}]}\\ J_{[\mu i][\nu j]} &\rightarrow J_{\mu[\nu+\boldsymbol{R}]},\end{aligned}$$

where $\boldsymbol{R} = (R_x,R_y,R_z)$ and $\boldsymbol{\tau}_\nu = (\tau_{\nu x},\tau_{\nu y},\tau_{\nu z})$ denote a lattice period and a basis vector of the unit cell, respectively. The lengths of the sublattice magnetic moments, $M_{\mu i} = M_\mu$ and $M_{\nu j} = M_\nu$, are the concentration weighted averages of the Fe and Co magnetic moments.

The dispersion curves for adiabatic linear spin waves are obtained by solving the eigenvalue problem for the eigenvalue $\epsilon_{\boldsymbol{q}n}$ ($\boldsymbol{q}$ wave vector, n band index) and associated eigenvector $v_{\mu\boldsymbol{q}n}$ [37],

$$v_{\mu\boldsymbol{q}n}\epsilon_{\boldsymbol{q}n} = 2g\mu_{\text{B}}\sum_\nu (M_\mu M_\nu)^{-\frac{1}{2}} v_{\nu\boldsymbol{q}n}\tilde{J}^{\mu\nu}_{\boldsymbol{q}}, \qquad (4)$$

where $\tilde{J}^{\mu\nu}_{\boldsymbol{q}}$ is short hand for

$$\tilde{J}^{\mu\nu}_{\boldsymbol{q}} \equiv J^{\mu\nu}_{\boldsymbol{q}} - \delta_{\mu\nu}\sum_\lambda J^{\lambda\mu}_0. \qquad (5)$$

The electron spin g-factor g is assumed to be 2 in the following. The Fourier transformed exchange interactions $J^{\mu\nu}_{\boldsymbol{q}}$ are defined by ($J^{\mu\nu}_0 \equiv J^{\mu\nu}_{\boldsymbol{q}=\boldsymbol{0}}$)

$$J^{\mu\nu}_{\boldsymbol{q}} = \delta_{\mu\nu}J_{\mu\mu} - \sum_{\boldsymbol{R}} J_{\mu[\nu+\boldsymbol{R}]}e^{i\boldsymbol{q}(\boldsymbol{\tau}_\mu-\boldsymbol{\tau}_\nu-\boldsymbol{R})}. \qquad (6)$$

Here, $J_{\mu\mu}$ is formally introduced since the lattice sum includes $\boldsymbol{R} = \mathbf{0}$ ($J_{\mu\mu} = 0$). All pair interactions within a shell of diameter $\approx 8a$ entered the Fourier transform.

III. RESULTS AND DISCUSSION

A. Structure of strained Fe-Co films

Structural optimization of the bct axial ratio c/a was performed for lattice parameters a in the interval 2.55 Å $\leqslant a \leqslant$ 2.80 Å. The present results for chemically homogeneous alloys shown in Fig. 1 are similar to those of our previous study [3] using the VCA and are only briefly discussed here. Figure 1 indicates that the tetragonality of the corresponding relaxed structures varies within $\sqrt{2} > c/a > 1$, i.e., in between the fcc and bcc boundaries. For all considered concentrations, the dependence of the relaxed c/a ratio on a follows approximately the one assuming a constant unit cell volume. We found that there is only a small compositional effect on the relaxed c/a ratio but for $a = 2.55$ Å and thus expect that volume effects (varying composition, a fixed) on the magnetic properties of bct $Fe_{1-x}Co_x$ are negligible but for $a = 2.55$ Å. We notice that the insensitivity of the c/a ratio on the Co content was experimentally validated for coherently grown bct $Fe_{1-x}Co_x$ ($0.4 \leqslant x \leqslant 0.6$) films on Rh(001) [7,8].

Investigations for partially and fully ordered alloys were performed for $Fe_{0.5}Co_{0.5}$ and $Fe_{0.4}Co_{0.6}$ in the range 2.60 Å $\leqslant a \leqslant$ 2.75 Å, i.e., the region with the highest predicted and measured uniaxial magnetic anisotropy [2–10]. In the present study, the sublattice concentration variable y was varied in the entire range, i.e., from $y = 0$ to $y = 0.5$ and to $y = 0.4$ for Co concentrations $x = 0.5$ and $x = 0.6$, respectively. The employed geometries for partially and fully ordered alloys are the ones for the homogeneous disordered alloy, because our calculations revealed that structural optimization of the c/a ratio as a function of the sublattice concentration y leads to a less than 1 % absolute change in the c/a ratio with respect to the homogeneously disordered alloy.

B. Curie temperature

The computed Curie temperature of $Fe_{1-x}Co_x$ films shows a strong dependence on tetragonality on the iron rich side that gradually weakens as more Co is alloyed to Fe; see the contour map $T_C(x,a)$ in Fig. 2(a). The iron rich corner ($Fe_{0.7}Co_{0.3}$ alloy) with tetragonality $c/a \approx 1.4$ exhibits the lowest Curie point on this map. An analysis of the exchange interactions revealed that antiferromagnetic interactions ($J < 0$) between Fe atoms in neighbor shells with coordinates (in units of the bct lattice parameters) (101), $(\frac{1}{2}\frac{3}{2}\frac{1}{2})$, and (201) appear, which is likely a precursor to the instability of ferromagnetic order in fcc iron. In contrast to the iron rich side, T_C is only moderately structure dependent on the Co rich side, e.g., T_C of $Fe_{0.2}Co_{0.8}$ varies by only 250 K in the entire considered a interval. We attribute this finding to the strong ferromagnetic behavior of $Fe_{0.2}Co_{0.8}$, i.e., a result of the virtually fully occupied d-majority spin band. Notice that ferromagnetic order is stable in fcc and bcc Co [42]. Strikingly, the Curie temperature of bct Fe-Co for 2.68 Å $\leqslant a \leqslant$ 2.75 Å ($1.14 \geqslant c/a \geqslant 1.08$) is largely *independent* on the composition.

As regards the Co effect on T_C of bcc Fe (experimental value 1043 K [1]) and the Fe effect on the T_C of fcc Co (experimental value 1388 K [1]), we found that our results are consistent with accessible experimental data and a previous theoretical analysis [1,43]. Accordingly, Co raises the Curie point of bcc Fe to a peak of ∼1600 K for $x \sim 30$ % [43]. On the other hand, Fe was found to decrease T_C of fcc Co by ~ -9 K per at. % Fe reaching ∼1160 K for fcc $Fe_{0.25}Co_{0.75}$ [1]. The latter value is close to our computed value (Fig. 2, lower limit on a), while we also find that T_C of $Fe_{0.7}Co_{0.3}$ approximates 1600 K as $c/a \to 1$ (Fig. 2, upper limit on a).

Turning to partially and fully ordered alloys, we found that the compositional and structural trends of T_C for $Fe_{0.5}Co_{0.5}$ and $Fe_{0.4}Co_{0.6}$ are similar; see the contour maps $T_C(y,a)$

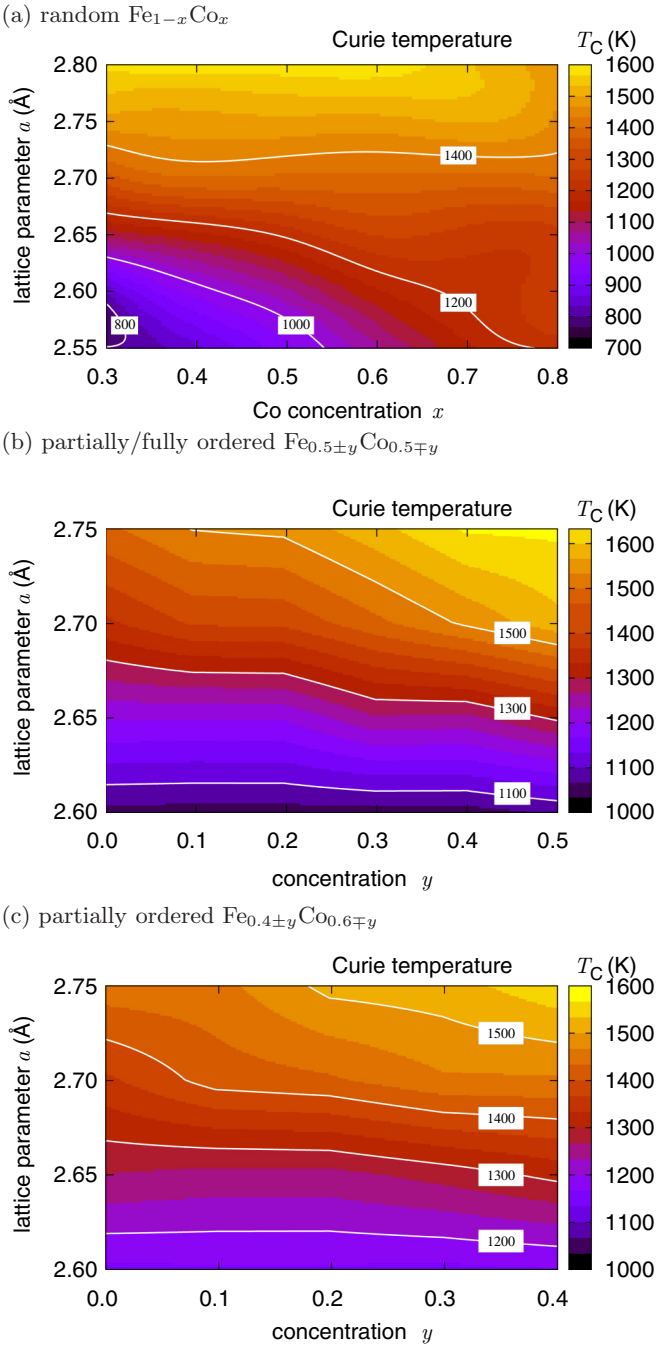

FIG. 2. Curie temperature of (a) homogeneously random $Fe_{1-x}Co_x$ alloy as a function of Co concentration x and lattice parameter a, and of partially or fully ordered (b) $Fe_{0.5\pm y}Co_{0.5\mp y}$ and (c) $Fe_{0.4\pm y}Co_{0.6\mp y}$ as a function of the sublattice concentration variable y and lattice parameter a. Notice the different range of the color scales.

shown in Figs. 2(b) and 2(c). An increase of the degree of ALRO tends to raise the Curie point. This effect is most pronounced for systems exhibiting the largest lattice parameter a (corresponding to the smallest tetragonality). Consequently, the already strong dependence of $T_C(y,a)$ on tetragonality for the homogeneously random alloys becomes even more pronounced toward the more ordered configurations.

In an attempt to shed light on the higher Curie temperature in the more ordered state, we consider two extreme scenarios in the following. The first scenario assumes that ALRO mainly enhances the magnitude of exchange interactions in Fe-Co as a whole, thereby raising T_C. This is immediately plausible from the mean-field picture for a monoatomic system where $T_C^{mf} \propto -J_0$ (for more than one sublattice, the mean-field estimate is proportional to the largest eigenvalue of a matrix spanned by $-J_0^{\mu\nu}$ [44]). The other extreme assumes that atomic order itself drives the variation of the Curie temperature due to different atomic distributions in coordination shells (order has a negligible effect on the J_{ij} in this scenario). In order to elucidate the latter case, we performed additional calculations of T_C for maximally ordered Fe-Co alloy using the exchange interactions obtained in the random state. These values for T_C are listed in Table I together with those for random alloys and alloys possessing the maximum degree of long-range order compatible with the concentration x. Accordingly, maximizing the ALRO while fixing the exchange interactions yields Curie temperatures slightly beyond those for the partially or fully ordered alloys. In other words, the increase of T_C due to increasing the ALRO towards B2 is mainly due to atomic order itself. The ordering effect on the magnitude of exchange interactions (as a whole) is weaker and actually results in a decrease of T_C if measured with respect to values obtained for ordered alloys using the exchange interactions obtained in the random state; see Table I.

It is worth addressing the important role of the tetragonality on T_C further. To this end, we analyzed the effective exchange interactions of the nearest-neighbor (NN) shells for all considered alloy configurations. We found that the present system is characterized by strong NN ferromagnetic interactions ($J > 0$) in the first coordination sphere (coordinates $(\frac{1}{2}\frac{1}{2}\frac{1}{2})$, eight NNs), weaker and damped interactions of either sign for larger interatomic distances (examples for exchange interactions are shown in Sec. III D; for a more detailed discussion of the exchange interactions in itinerant ferromagnets, their long-ranged and oscillatory character (Ruderman-Kittel-Kasuya-Yoshida behavior), as a function of interatomic separation, we refer the reader to, e.g., Turek *et al.* [45]). Interestingly, we found that the c/a dependence of the first NN interaction J_{1NN} is consistent with the one of T_C, i.e., J_{1NN} decreases monotonically as a function of decreasing a (increasing c/a ratio) in $Fe_{1-x}Co_x$ for all considered x, and in partially or fully ordered $Fe_{0.5\pm y}Co_{0.5\mp y}$ and $Fe_{0.4\pm y}Co_{0.6\mp y}$ for all considered y (not shown). Because of these correlations and the dominance of J_{1NN}, judged in due consideration of the number of equivalent neighbors, we reason that J_{1NN} plays the most decisive role for the dependence of T_C on tetragonal distortion. A similar correlation between J_{1NN} and T_C was reported in earlier work for bct B2 ordered FeCo compound [46].

TABLE I. ALRO effect on the Curie temperature: listed are T_C for random alloy (third column), partially or fully ordered Fe-Co alloy with maximum degree of long-range order (forth column), and partially or fully ordered Fe-Co alloy using the exchange interactions (generic symbol J) obtained in the random state (last column).

		Random J $y = 0$	Max. ordered J max y	Random J max y
x	a (Å)		T_C (K)	
0.5	2.65	1207	1309	1345
	2.75	1457	1606	1625
0.6	2.65	1254	1316	1327
	2.75	1453	1550	1557

C. Spin-wave dispersion

The spin-wave energies $\epsilon_{\boldsymbol{q}n}$ are functions of the Fourier transformed $J_{\mu[\nu+\boldsymbol{R}]}$, i.e., the complexity of the real space exchange interactions reflects in complex features of $\epsilon_{\boldsymbol{q}n}$. Specifying the eigenvalue problem Eq. (4) for the present case of two sublattices ($\mu,\nu = \{1,2\}$), nontrivial solutions are obtained for eigenenergies

$$\epsilon_{\boldsymbol{q}\pm}^2 - 4\mu_B\left(\frac{\tilde{J}_{\boldsymbol{q}}^{11}}{M_1} + \frac{\tilde{J}_{\boldsymbol{q}}^{22}}{M_2}\right)\epsilon_{\boldsymbol{q}\pm} + (4\mu_B)^2\left(\frac{\tilde{J}_{\boldsymbol{q}}^{11}\tilde{J}_{\boldsymbol{q}}^{22} - \tilde{J}_{\boldsymbol{q}}^{12}\tilde{J}_{\boldsymbol{q}}^{21}}{M_1 M_2}\right) = 0. \quad (7)$$

In the case of random alloys, the two sublattices are identical and the eigenvalue problem may be reduced to the primitive unit cell containing one site, hence to one spin-wave branch. Here we work, however, with the conventional unit cell (two sites) in order to ease the comparison to partially or fully ordered alloys (with two "true" sublattices).

In Figs. 3(a) and 3(b), we present a detailed analysis of the computed spin-wave spectra for two distinct bct geometries and varying Co concentration, $x = \{0.3,0.5,0.8\}$. All spectra deviate from a simple cosine shape along the $\Gamma - Z$, $\Gamma - X$, and $\Gamma - M$ high symmetry directions, indicating important interactions with several coordination shells. In one case, $a = 2.65$ Å ($c/a \approx 1.20$–1.21) shown in Fig. 3(b), increasing Co concentration mainly broadens the bandwidth of the spin-wave spectrum and raises the zone boundary eigenenergies. The associated increase in slope of the $\epsilon_{\boldsymbol{q}}$ curve near Γ is not isotropic in $\boldsymbol{q}$ space and the eigenenergy at the M point rises more strongly than at Z. While for $a = 2.55$ Å ($c/a \approx 1.36$–1.41) shown in Fig. 3(a) the impact of Co on the spin-wave bandwidth is even more pronounced, also a qualitative shift of the dispersion curves occurs when the eigenenergy of the optical branch at Γ softens below the maximum spin-wave energy not coinciding with any high-symmetry point. This transition occurs upon reducing x at approximately equiconcentration is connected with the appearance of antiferromagnetic exchange interactions with the neighbor shells with coordinates (101) and $(\frac{1}{2}\frac{3}{2}\frac{1}{2})$. Notice that $c/a \approx 1.41$ for $a = 2.55$ Å in $Fe_{0.7}Co_{0.3}$ (cf. Fig. 1) and that this composition possesses a very low Curie temperature (cf. Sec. III B).

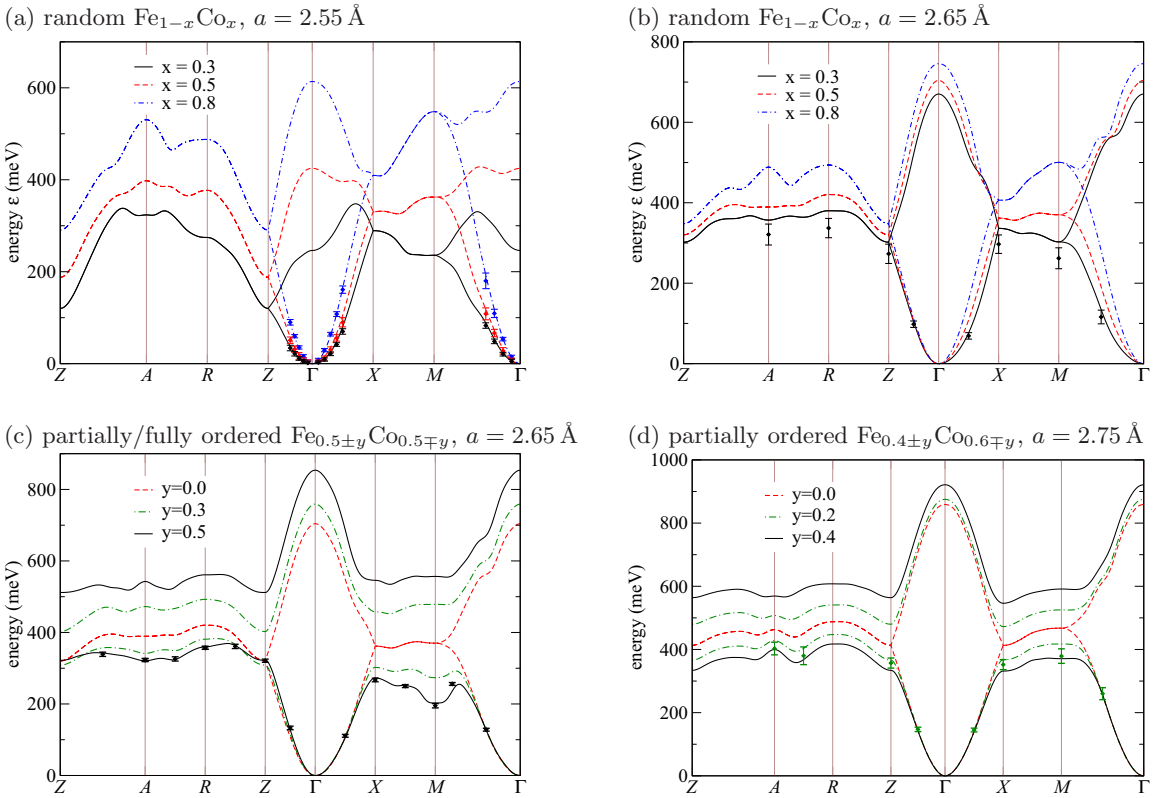

FIG. 3. Spin-wave dispersion relations between high-symmetry points in the Brillouin zone for random $Fe_{1-x}Co_x$ for (a) $a = 2.55$ Å and (b) $a = 2.65$ Å and selected Co concentrations, and for partially or fully ordered (c) $Fe_{0.5\pm y}Co_{0.5\mp y}$ at $a = 2.65$ Å and (d) $Fe_{0.4\pm y}Co_{0.6\mp y}$ at $a = 2.75$ Å. The points mark spin-wave dispersion relations obtained from the dynamical structure factor $S^k(\boldsymbol{q},\omega)$ by means of atomistic spin-dynamics simulations (details see text). The corresponding error bars are a measure of spin-wave damping (FWHM of the spectral function).

The Co effect on the spin-wave properties of bct $Fe_{1-x}Co_x$ may be understood by uncovering the convergence of $\epsilon_{\boldsymbol{q}}$ at high-symmetry points as a function of the number of coordination shells included in the lattice summation in Eq. (6). From the data for $Fe_{1-x}Co_x$, $x = \{0.3,0.5,0.8\}$, and at $a = 2.65$ Å shown in Table II, several important conclusions can be drawn. As previously discussed, $J_{1\mathrm{NN}}$ is the largest and consequently determines the order of magnitude of the spin-wave bandwidth. The chemical trend of the converged $\epsilon_{\boldsymbol{q}}$ at high-symmetry points as a function of increasing Co concentration is not reflected in the magnitude of $J_{1\mathrm{NN}}$, which decreases with Co addition (indicated by the smaller bandwidth taken into account only the first coordination shell). Extending the lattice summation to the first six coordination shells already describes the observed *chemical trend* reasonably well, although most eigenenergies of zone-boundary modes and at Γ approach the converged values at longer range.

The dependence of the spin-wave dispersion relations on ALRO in the Fe-Co alloy is detailed in Fig. 3(c) for $Fe_{0.5\pm y}Co_{0.5\mp y}$ (at $a = 2.65$ Å) and in Fig. 3(d) for $Fe_{0.4\pm y}Co_{0.6\mp y}$ (at $a = 2.75$ Å, $c/a \approx 1.07$–1.08). The primary consequence of forming two distinct magnetic sublattices is a lifted degeneracy at the zone boundary and the opening of a gap that separates the acoustic from the optical spin-wave branch. In both cases, the band gaps are the largest for the upper limit on y but may not form symmetrically with respect to the $y = 0$ energies. In particular for $Fe_{0.4\pm y}Co_{0.6\mp y}$, the bands are quite dispersion-less along the zone boundary. A secondary result of the increasing degree of long-range order, i.e., toward

TABLE II. Eigenenergies $\epsilon_{\boldsymbol{q}}$ (in units of meV) at high-symmetry points of the Brillouin zone taken into account exchange interactions for the first and first six coordination shells and considering the maximum number of computed exchange interactions for bct $Fe_{1-x}Co_x$ with $a = 2.65$ Å. The first six shell coordinates (for $1 \leqslant c/a < \sqrt{2}$) in units of the bct lattice parameters with the number of equivalent sites in square brackets are: $(\frac{1}{2}\frac{1}{2}\frac{1}{2})$[8], (100) [4], (001) [2], (110) [4], (101) [8], and $(\frac{1}{2}\frac{3}{2}\frac{1}{2})$ [16].

x	0.3			0.5			0.8		
shells	One	Six	Max	One	Six	Max	One	Six	Max
$\boldsymbol{q}$-point									
Z $(00\frac{1}{2})$	333	334	302	321	372	320	304	427	348
A $(\frac{1}{2}\frac{1}{2}\frac{1}{2})$	333	369	357	321	415	389	304	508	489
R $(0\frac{1}{2}\frac{1}{2})$	333	387	380	321	435	420	304	502	494
Γ (000)[a]	666	616	670	642	669	704	608	744	746
X $(\frac{1}{2}00)$	333	350	336	321	400	362	304	475	406
M $(\frac{1}{2}\frac{1}{2}0)$	333	320	303	321	384	370	304	509	500

[a]Optical branch.

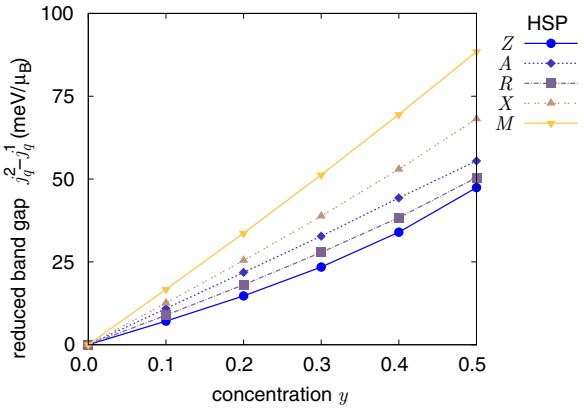

FIG. 4. Reduced band gap [Eq. (8)] at various high-symmetry points (HSP) as a function of the sub-lattice concentration variable y for $Fe_{0.5\pm y}Co_{0.5\mp y}$ and $a = 2.65$ Å. Lines guide the eye.

a configuration with on average chemically distinct nearest neighbors, is an increase of the spin-wave bandwidth at Γ.

The zone-boundary band gap, $\Delta\epsilon_{\boldsymbol{q}} = \epsilon_{\boldsymbol{q}+} - \epsilon_{\boldsymbol{q}-}$, where $\tilde{J}_{\boldsymbol{q}}^{12} = \tilde{J}_{\boldsymbol{q}}^{21} = 0$, may simply be obtained via

$$\frac{\Delta\epsilon_{\boldsymbol{q}}}{4\mu_{\mathrm{B}}} = \left|j_{\boldsymbol{q}}^2 - j_{\boldsymbol{q}}^1\right|, \quad j_{\boldsymbol{q}}^{\mu} \equiv \frac{\tilde{J}_{\boldsymbol{q}}^{\mu\mu}}{M_{\mu}}. \tag{8}$$

The analysis of $j_{\boldsymbol{q}}^2 - j_{\boldsymbol{q}}^1$ for $Fe_{0.5\pm y}Co_{0.5\mp y}$ shows that this difference is positive definite at all high-symmetry points of the Brillouin zone and increases monotonically as a function of y; see Fig. 4. The relation between band gap and y is approximately linear but at the Z point. The positive definiteness of $j_{\boldsymbol{q}}^2 - j_{\boldsymbol{q}}^1$ implies that the Fourier transformed effective exchange interactions of the Co-rich sub-lattice ($\tilde{J}_{\boldsymbol{q}}^{22}$) exceed the magnitude of the Fourier transformed Fe-rich intrasublattice interactions ($\tilde{J}_{\boldsymbol{q}}^{11}$), although $\tilde{J}_{\boldsymbol{q}}^{11}$ is normalized by a larger moment on the iron-rich sites than $\tilde{J}_{\boldsymbol{q}}^{22}$ is on the cobalt-rich sub-lattice, i.e., $M_1 > M_2$.

The overall energetic lowering of the acoustic spin-wave branch in the more ordered alloy configurations (shift of the acoustic spin-wave density of states to lower energies) makes acoustical spin-wave modes more easily excitable as long as spin-wave interactions can be neglected. The ALRO effect on long wavelength acoustic spin-waves is considered in detail in Sec. III D.

Finally, we investigate selected spin-wave dispersion relations by means of atomistic spin-dynamics simulations without resorting to the VCA average for the randomness in the exchange interactions [Eq. (2)]. The atomistic spin-dynamics approach to the adiabatic spin-wave spectrum has been elaborately described in the literature [47–50] and is only briefly outlined here. The starting point is the temporal evolution of the spin moments $\mathbf{e}_i$ in Eq. (1) at finite temperatures, which is governed by Langevin dynamics through coupled stochastic differential equations (Landau-Lifschitz-Gilbert equations). The fundamental quantity of interest for the adiabatic spin-wave spectrum is the dynamical structure factor $S^k(\boldsymbol{q},\omega)$ ($\omega = 2\pi\upsilon$), which is the Fourier transformed space- and time-displaced spin-spin correlation function [48,49]. The spin-wave dispersion relations may be determined from the peak position of the structure factor along a $\boldsymbol{q}$-vector path [38,47,49]. Here, we used UppAsd to calculate $S^k(\boldsymbol{q},\omega)$ and focus only on alloy disorder-induced spin-wave damping. To this end, we fixed the simulation temperature $T = 1$ K and Gilbert damping constant $\alpha = 0.001$ in order to minimize other broadening effects, similar to earlier work for Fe-Co [38]. As a measure of the alloy-disorder effect we employed the full width at half maximum (FWHM) of the spectral function $S^k(\boldsymbol{q},\omega)$.

The results of the atomistic spin-dynamics simulations are also shown in Figs. 3(a)–3(d). In comparison to the adiabatic spin-wave curves derived from Eq. (7) (acoustic branch), the main conclusions are that (*i*) the adiabatic spin-wave spectrum of ordered FeCo is well captured [Fig. 3(c)], (*ii*) the agreement for long wavelengths, where peak broadening due to alloy disorder is small, is generally very good, (*iii*) spin-waves with shorter wavelength are more sensitive to local site disorder indicated by broader peaks, and (*iv*) a softening of spin-waves at high-symmetry points occurs. The latter two points indicate that the VCA average for the randomness in the exchange interactions is less reliable far from the Γ-point, where the spin-wave spectra of Fe-Co become more diffuse and life-time effects more significant.

D. Spin-wave stiffness and anisotropy

The spin-wave stiffness—the prefactor in the quadratic spin-wave dispersion relation on the acoustical branch in the long-wavelength limit—could be obtained from a fit to the spin-wave dispersion curves $\epsilon_{\boldsymbol{q}n}$. Due to the long-range oscillatory nature of the exchange interactions in the present alloy, $J_{\boldsymbol{q}}^{\mu\nu}$ converges, however, badly even for high $\boldsymbol{R}$ cutoff. To resolve the issue in obtaining reliable spin-wave stiffnesses, we applied a regularization procedure, originally proposed for Bravais lattices [51], to the spin-wave stiffness tensor $D^{\alpha\beta}$ derived in the Appendix. We replace Eq. (A7) by a formally identical expression

$$D^{\alpha\beta} = \lim_{\eta\to 0} D_{\eta}^{\alpha\beta}, \tag{9}$$

$$D_{\eta}^{\alpha\beta} = \frac{2\mu_{\mathrm{B}}}{M_1 + M_2} \sum_{\mu\nu} \sum_{\boldsymbol{R}} J_{\mu[\nu+\boldsymbol{R}]}(\tau_{\mu\alpha} - \tau_{\nu\alpha} - R_{\alpha}) \times (\tau_{\mu\beta} - \tau_{\nu\beta} - R_{\beta}) e^{-\eta|\boldsymbol{R}|/a}, \tag{10}$$

which yields numerically convergent spin-wave stiffnesses. We recently evaluated the numerical accuracy of this procedure to 2 meV Å^2 for bcc random $Fe_{0.9}Co_{0.1}$ alloy related to the choice of the damping parameter η [52] and found the same accuracy for the presently considered bct systems. In praxis, exchange pairs within a sphere of radius $\approx 8a$ were used for the computation of $D_{\eta}^{\alpha\beta}$, where η was varied within [0.8 : 1.1] and extrapolated to $\eta = 0$ using a second-order polynomial.

For the present tetragonal systems, $D^{\alpha\beta}$ has two distinct principal values, $D^{xx} = D^{yy}$ and D^{zz}. We concentrate on the scalar,

$$D = (D^{xx} D^{yy} D^{zz})^{1/3}, \tag{11}$$

which is the relevant prefactor in the temperature dependence of the spontaneous magnetization at low temperatures due to spin-wave excitations (Bloch's law) [53], and define the

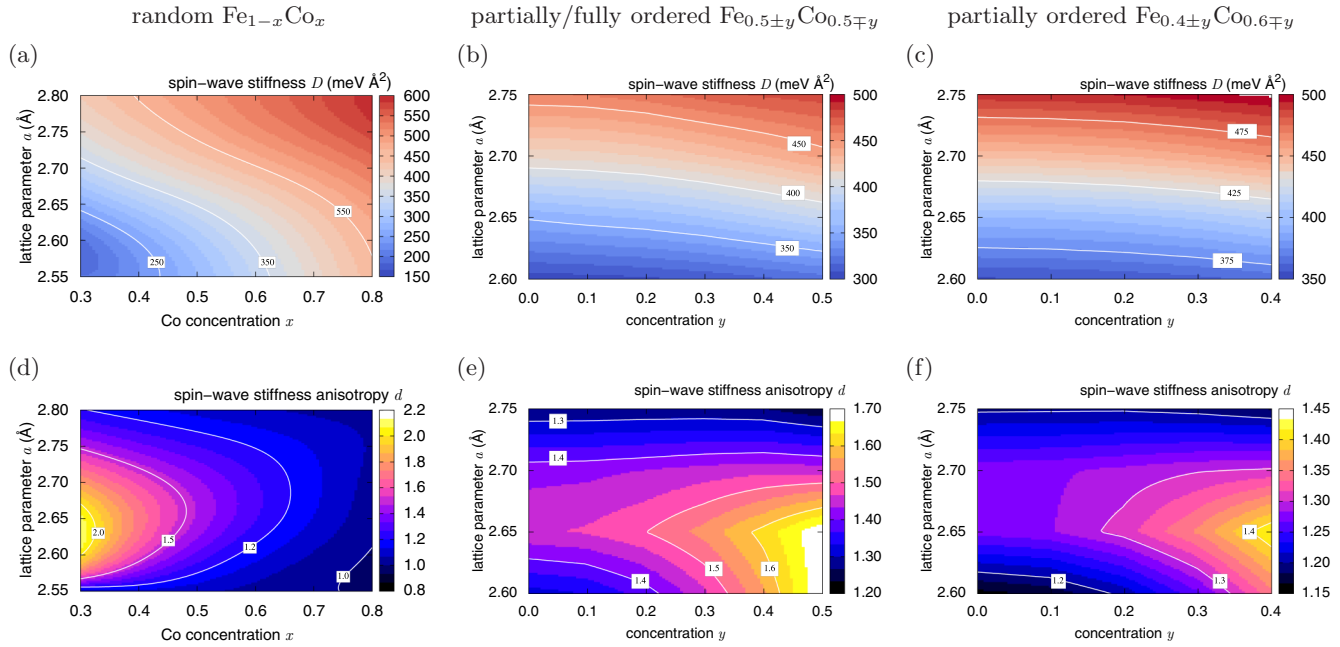

FIG. 5. Spin-wave stiffness (top row) and spin-wave stiffness anisotropy (bottom row) of homogeneously random $Fe_{1-x}Co_x$ alloy as a function of Co concentration x and lattice parameter a (left column), and of partially or fully ordered $Fe_{0.5\pm y}Co_{0.5\mp y}$ (center column) and $Fe_{0.4\pm y}Co_{0.6\mp y}$ (right column) as a function of the sublattice concentration variable y and lattice parameter a. Notice the different range of the color scales.

spin-wave stiffness anisotropy d from the principal values as

$$d \equiv \frac{D^{zz}}{D^{xx}}. \tag{12}$$

An anisotropy larger (smaller) than one means that long-wavelength acoustical spin waves with in-plane wave vectors are more (less) easily excited than spin waves with q parallel to the z axis. Notice that $d = 1$ if $c/a = 1$ (bcc) or $c/a = \sqrt{2}$ (fcc) by symmetry properties of the symmetrical second-rank tensor $D^{\alpha\beta}$ for cubic lattices.

The detailed analysis of the spin-wave stiffness for random $Fe_{1-x}Co_x$ films shows a strong dependence on both Co concentration and tetragonality; see the contour map $D(x,a)$ in Fig. 5(a). The iron-rich $Fe_{0.7}Co_{0.3}$ alloy with tetragonality $c/a \approx 1.4$ exhibits the softest spin-wave stiffness, while the maximum spin-wave stiffness occurs in the cobalt-rich and low c/a corner in this map. We omit presenting the compositional and structural trends of the two components $D^{xx}(x,a)$ and $D^{zz}(x,a)$ here and instead focus on and discuss their mutual ratio. $d(x,a)$ as shown in Fig. 5(d) reveals that $d > 1$ for most Co concentrations and lattice parameters a, i.e., acoustical spin waves with in-plane wave vectors are for most configurations (x,a) more easily excitable than waves with out-of-plane vector component. The anisotropy approaches, as expected, the symmetry dictated value of 1 in the limit of the smallest and largest a (i.e., on approaching the fcc and bcc boundaries, cf. Fig. 1), while the transition from $d > 1$ to $d < 1$ close to the $Fe_{0.2}Co_{0.8}$ alloy with $a = 2.55$ Å is not induced by lattice symmetry. The Fe-rich side of the map $d(x,a)$ exhibits a prominent peak of height $d \approx 2$ centered at $a \approx 2.63$ Å, which gradually disappears with more Co content in the matrix. This drop of d with x is also reflected in the curvature of $\epsilon_{\boldsymbol{q}}$ for $a = 2.65$ Å as shown in Fig. 3(b): $\epsilon_{\boldsymbol{q}}$ changes significantly along Γ-X in contrast to the nearly rigid curvature along Γ-Z. Notice that the peak maximum is approximately located at $c/a = (\sqrt{2}+1)/2$ possibly pointing to a geometric origin, i.e., the tetragonal lattice distortion deviates the most from cubic symmetry in the range $1 \leqslant c/a \leqslant \sqrt{2}$.

We found that the compositional and structural trends of $D(y,a)$ and $d(y,a)$ are rather similar for the two investigated partially or fully ordered alloys, see the two contour maps $D(y,a)$ shown in Figs. 5(b) and 5(c). Accordingly, an increase of the degree of ALRO increases the spin-wave stiffness, thus the excitation of long-wavelength acoustic spin waves in random configurations is easier than in the more ordered configurations. This effect is most pronounced for systems exhibiting the largest lattice parameter a and is reminiscent of the trend of the Curie point. For all degrees of atomic order, D exhibits a strong dependence on tetragonality. The spin-wave stiffness anisotropy $d(y,a)$ [Figs. 5(e) and 5(f)] is larger than one, peaks close to the lattice parameter $a = 2.65$ Å for all y, and increases strongly toward the maximum degree of ALRO except for the largest investigated a values. We notice that D and d computed from recently reported values on D^{xx} and D^{zz} for B2 ordered bct FeCo compound [23] are in close agreement with the present values, although experimental lattice parameters were assumed in the calculations of Ref. [23].

Both the pronounced peak in the concentration dependence of $d(x,a)$ and the strong atomic ordering effect on $d(y,a)$ in the present alloy system may be understood on the basis of the underlying pair exchange interactions. With intent to uncover the dominating physical mechanism *in the range of the NNs* only, we narrow the analysis of the exchange interactions to the first six shells. These are shown in Figs. 6(a) and 6(b) for bct random $Fe_{1-x}Co_x$ alloy, $x = \{0.3, 0.5, 0.8\}$, and two lattice

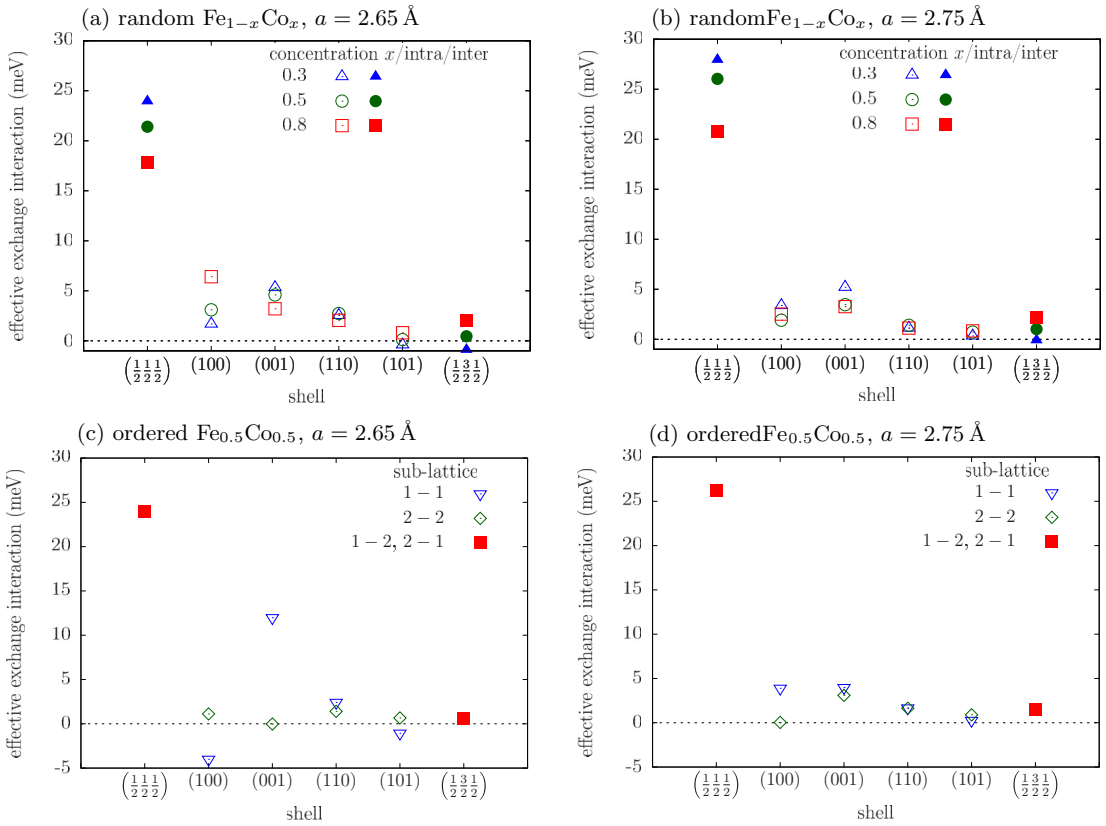

FIG. 6. Effective exchange interactions for the first six coordination shells (sorted in order of interatomic distance) of random bct $Fe_{1-x}Co_x$, $x = \{0.3,0.5,0.8\}$, for (a) $a = 2.65$ Å and (b) $a = 2.75$ Å. Exchange interactions for ordered FeCo ($x = y = 0.5$) are shown in (c) for $a = 2.65$ Å and in (d) for $a = 2.75$ Å. Open and filled symbols denote intra- and intersublattice interactions, respectively. Note that for the ordered alloy [panels (c) and (d)], sublattice "1" and "2" are pure Fe and Co, respectively.

parameters, $a = \{2.65\,\text{Å}, 2.75\,\text{Å}\}$. We recall that $d(x,a = 2.65\,\text{Å})$ shows the stronger x-dependence [Fig. 5(d)]. If we assume in the following that the summation over $\boldsymbol{R}$ in Eq. (A7) is performed coordination shell by coordination shell, then the contribution of the first NN shell to d is equal to $(c/a)^2$ for $1 \leqslant c/a < \sqrt{2}$,[1] thus does not depend on x. The particular concentration dependencies of $J_{2\text{NN}}$ and $J_{3\text{NN}}$ (third NNs interaction) introduce a difference to d: $J_{2\text{NN}}$ stiffens (softens) for $a = 2.65$ Å (for $a = 2.75$ Å) with increasing x, while $J_{3\text{NN}}$ softens in both cases [Figs. 6(a) and 6(b)]. Since $J_{2\text{NN}}$ updates only D^{xx} and $J_{3\text{NN}}$ only D^{zz}, both shells lead a strong dependence and a weak dependence of $d(x,a)$ on x for $a = 2.65$ Å and $a = 2.75$ Å, respectively. The influence of composition on the fourth to sixth NN shells are comparable in both cases.

The ordering effect on $d(y,a)$ can then be understood by comparing the exchange interactions in the ordered state, Figs. 6(c) and 6(d), to the ones in the random state, Figs. 6(a) and 6(b). This might be done by looking at the arithmetic average since the intrasublattice interactions on the Fe and Co sublattices, in particular, for the shells (100) and (001) in the case $a = 2.65$ Å and for (100) in the case $a = 2.75$ Å differ significantly from each other. Beyond the first NN shell and for $a = 2.75$ Å, we found that the arithmetic averages of the intrasublattice interactions (shells 2–5) and the intersublattice interaction with the sixth NN shell in ordered states are quite similar to their counterparts in the random state. Hence, the shell-wise updates of d do not differ substantially. For $a = 2.65$ Å, the average (100) and (001) interactions in the ordered state are, however, notably smaller and larger, respectively, than in the random state and mainly responsible for the increase of d with concentration.

[1]Notice that $d = 1$ for $c/a = \sqrt{2}$ because there are 12 sites in the first coordination shell.

IV. CONCLUSIONS

Ab initio alloy theory as formulated in the coherent-potential approximation and implemented in the EMTO code was employed to describe geometry and interatomic magnetic exchange interactions of homogeneously disordered, partially and fully ordered $Fe_{1-x}Co_x$ alloy films ($0.3 \leqslant x \leqslant 0.8$). The body-centered tetragonal structure of the strained films was modeled in the framework of the epitaxial Bain path, which established a relation between the relaxed out-of-plane lattice parameter as a function of in-plane strain. The degree of atomic long-range order was found to have a negligible influence on the relaxed out-of-plane lattice parameter. A nonrelativistic Heisenberg model parameterized with the computed exchange interactions was used to estimate the Curie temperature of the alloy in conjunction with Monte Carlo simulations. The dependence of the Curie temperature for homogeneously

random configurations on alloy composition and in-plane lattice parameter results from a pronounced dependence on tetragonality, strong ferromagnetism in the Co-rich alloy, and the beginning instability of ferromagnetic order in $Fe_{0.7}Co_{0.3}$ when $c/a \to \sqrt{2}$ (face-centered cubic structure). Increasing atomic long-range order was found to raise the Curie point and originates mainly from the order itself, i.e., different distributions of atoms in neighboring coordination shells rather than an intrinsic alteration of exchange interactions.

The spin-wave dynamics was addressed within the adiabatic theory where the randomness in the exchange integrals was treated in the virtual-crystal approximation. The discussed spin-wave spectra deviate from a simple cosine shape and their bandwidths increase with the amount of Co and the degree of atomic long-range order. The maximum spin-wave energies are roughly five to six times higher than the Curie temperature and are thus expected to be occupied sparsely at T_C. In order to test the reliability of the virtual-crystal approximation to the randomness in the exchange integrals for Fe-Co, we computed selected spin-wave spectra (acoustic branch) by means of atomistic spin-dynamics simulations for the alloy Hamiltonian Eq. (1) and subsequent analysis of the dynamical structure factor. The results indicate that the virtual-crystal approximation is less reliable far from the Γ point, where local site disorder broadens and softens the spin-wave spectra. The agreement between both approaches is, however, close for long wavelengths.

Our results indicate that long-wavelength spin-wave excitations as characterized by the spin-wave stiffness show overall similar dependencies on x and a as T_C. The correlation is particularly strong as regards the effect of atomic long-range order on D. The directional anisotropy of the spin-wave stiffness for the random Fe-Co alloy indicates that acoustical spin waves with in-plane wave vector are for most configurations (x,a) more easily excitable than waves with out-of-plane vector component. The spin-wave anisotropy was found to exhibit a prominent peak in narrow ranges of concentration and tetragonality, and a strong long-range order effect on the anisotropy was observed for near equiconcentration Fe-Co alloy and particular geometries. Sources to both findings could be traced back to exchange interactions at the near and intermediate ranges.

What is more, atomic long-range order was predicted as a means to tune both the Curie temperature and the spin-wave dynamics. Experimentally, a variation of atomic long-range order in Fe-Co can be achieved by varying the annealing temperature and the annealing time in quenched samples [54]. The maximum computed ordering effects on T_C and D are about 10% and approximately 20% in the case of d. Small perturbations of the maximum order yield small variations of T_C and D. In contrast, the previously reported atomic long-range order effect on the magnetocrystalline anisotropy energy of Fe-Co [3,4] is much more significant and already small deviations from maximum order can have a detrimental effect on the anisotropy energy.

With regard to utilizing $Fe_{1-x}Co_x$ alloys for perpendicular magnetic recording applications, our results indicate that both the alloy composition and the substrate lattice parameter in coherent epitaxial growth of Fe-Co films are similarly effective factors in tailoring Curie temperature and spin-wave dynamics as is atomic long-range order. It seems that controlling the atomic long-range order is the most important factor for achieving high values of the magnetocrystalline anisotropy energy since the appearance of a perpendicular easy axis is confined to relatively narrow ranges of alloy composition and tetragonality.

Future studies could elucidate the ordering effect on the fundamental magnetic properties of alloys, which are composed of species with dissimilar pair exchange interactions.

ACKNOWLEDGMENTS

Fruitful discussions with Lars Bergqvist are gratefully acknowledged. Financial support by the Swedish Research Council, the Swedish Foundation for Strategic Research, the Swedish Foundation for International Cooperation in Research and Higher Education, the Carl Tryggers Foundation for Scientific Research, the Chinese Scholarship Council, and the Hungarian Scientific Research Fund (OTKA Grants No. 84078 and No. 109570) are gratefully acknowledged. The Swedish National Infrastructure for Computing at the National Supercomputer Centers in Linköping and Stockholm are acknowledged for providing computational facilities.

APPENDIX: SPIN-WAVE STIFFNESS TENSOR

Expanding the exponential in Eq. (6) in the limit $\boldsymbol{q} \to \boldsymbol{0}$ [$\boldsymbol{q} = q\hat{\boldsymbol{q}}$, $|\hat{\boldsymbol{q}}| = 1$, $\hat{\boldsymbol{q}} = (\hat{q}_x,\hat{q}_y,\hat{q}_z)$] yields

$$e^{i\boldsymbol{q}\boldsymbol{r}} \approx 1 + iq\hat{\boldsymbol{q}}\boldsymbol{r} - \tfrac{1}{2}q^2(\hat{\boldsymbol{q}}\boldsymbol{r})^2 + \mathcal{O}[(\boldsymbol{q}\boldsymbol{r})^3]. \tag{A1}$$

Using this expansion in combination with symmetries of lattice and exchange interactions, $\tilde{J}^{\mu\nu}_{\boldsymbol{q}}$ [Eq. (5)] can then be cast into

$$\tilde{J}^{\mu\nu}_{\boldsymbol{q}} \approx J^{\mu\nu}_0 - \delta_{\mu\nu}\sum_{\lambda} J^{\lambda\mu}_0 + \hat{J}^{\mu\nu}_{\hat{\boldsymbol{q}}} q^2, \tag{A2}$$

where we defined $\hat{J}^{\mu\nu}_{\hat{\boldsymbol{q}}}$ as

$$\hat{J}^{\mu\nu}_{\hat{\boldsymbol{q}}} \equiv \frac{1}{2}\sum_{\boldsymbol{R}} J_{\mu[\nu+\boldsymbol{R}]}[\hat{\boldsymbol{q}}(\boldsymbol{\tau}_\mu - \boldsymbol{\tau}_\nu - \boldsymbol{R})]^2. \tag{A3}$$

With $\tilde{J}^{\mu\nu}_{\boldsymbol{q}}$ from Eq. (A2), the two solutions of Eq. (7) are of the form

$$\epsilon_{\boldsymbol{q}\pm} = 2\mu_B\left(-A + Bq^2 \pm \sqrt{A^2 + Cq^2 + Dq^4}\right), \tag{A4}$$

of which $\epsilon_{\boldsymbol{q}-}$ correspond to the acoustic mode. A final Taylor expansion of the square-root term in the previous expression in terms of q^2 up to first order yields

$$\epsilon_{\boldsymbol{q}-} = \frac{4\mu_B}{M_1 + M_2}\sum_{\mu\nu}\hat{J}^{\mu\nu}_{\hat{\boldsymbol{q}}} q^2 \tag{A5}$$

valid for the acoustic mode and $\boldsymbol{q} \to \boldsymbol{0}$.

The components of the spin-wave stiffness tensor $D^{\alpha\beta}$ are derived from

$$D^{\alpha\beta} = \frac{1}{2q^2}\frac{\partial^2\epsilon_{\boldsymbol{q}-}}{\partial\hat{q}_\alpha\partial\hat{q}_\beta} \quad \alpha,\beta = \{x,y,z\}, \tag{A6}$$

$$= \frac{2\mu_B}{M_1 + M_2}\sum_{\mu\nu}\sum_{\boldsymbol{R}} J_{\mu[\nu+\boldsymbol{R}]}(\tau_{\mu\alpha} - \tau_{\nu\alpha} - R_\alpha) \times (\tau_{\mu\beta} - \tau_{\nu\beta} - R_\beta), \tag{A7}$$

which is the desired result.

[1] Edited by H. P. J. Wijn, *Magnetic Properties of Metals* (Springer-Verlag, Berlin, Heidelberg, 1991).

[2] T. Burkert, L. Nordström, O. Eriksson, and O. Heinonen, Phys. Rev. Lett. **93**, 027203 (2004).

[3] C. Neise, S. Schönecker, M. Richter, K. Koepernik, and H. Eschrig, Phys. Status Solidi B **248**, 2398 (2011).

[4] I. Turek, J. Kudrnovský, and K. Carva, Phys. Rev. B **86**, 174430 (2012).

[5] Y. Kota and A. Sakuma, Appl. Phys. Express **5**, 113002 (2012).

[6] A. Winkelmann, M. Przybylski, F. Luo, Y. Shi, and J. Barthel, Phys. Rev. Lett. **96**, 257205 (2006).

[7] F. Luo, X. L. Fu, A. Winkelmann, and M. Przybylski, Appl. Phys. Lett. **91**, 262512 (2007).

[8] F. Yildiz, F. Luo, C. Tieg, R. M. Abrudan, X. L. Fu, A. Winkelmann, M. Przybylski, and J. Kirschner, Phys. Rev. Lett. **100**, 037205 (2008).

[9] F. Yildiz, M. Przybylski, X.-D. Ma, and J. Kirschner, Phys. Rev. B **80**, 064415 (2009).

[10] H. Oomiya, B. Wang, S. Yoshida, T. Kataguchi, K. Takahashi, S. Kanatani, L. Zhang, L. Liu, T. Hasegawa, K. Hayasaka, S. Saito, N. Inami, T. Ueno, K. Ono, and S. Ishio, J. Phys. D: Appl. Phys. **48**, 475003 (2015).

[11] J. Buschbeck, I. Opahle, M. Richter, U. K. Rößler, P. Klaer, M. Kallmayer, H. J. Elmers, G. Jakob, L. Schultz, and S. Fähler, Phys. Rev. Lett. **103**, 216101 (2009).

[12] S. Kauffmann-Weiss, S. Hamann, L. Reichel, A. Siegel, V. Alexandrakis, R. Heller, L. Schultz, A. Ludwig, and S. Fähler, APL Mater. **2**, 046107 (2014).

[13] S. Schönecker, M. Richter, K. Koepernik, and H. Eschrig, New J. Phys. **17**, 023005 (2015).

[14] S. Okamoto, N. Kikuchi, O. Kitakami, T. Miyazaki, Y. Shimada, and K. Fukamichi, Phys. Rev. B **66**, 024413 (2002).

[15] J. B. Staunton, S. Ostanin, S. S. A. Razee, B. Gyorffy, L. Szunyogh, B. Ginatempo, and E. Bruno, J. Phys.: Condens. Matter **16**, S5623 (2004).

[16] C. J. Aas, L. Szunyogh, J. S. Chen, and R. W. Chantrell, Appl. Phys. Lett. **99**, 132501 (2011).

[17] M. L. Plumer, J. van Ek, and D. Weller, eds., *The Physics of Ultra-High-Density Magnetic Recording* (Springer-Verlag, Berlin, Heidelberg, New York, 2001).

[18] T. W. McDaniel, J. Phys.: Condens. Matter **17**, R315 (2005).

[19] M. H. Kryder, E. C. Gage, T. W. McDaniel, W. A. Challener, R. E. Rottmayer, G. Ju, Y.-T. Hsia, and M. Fatih Erden, Proc. IEEE **96**, 1810 (2008).

[20] T. J. Silva, P. Kabos, and M. R. Pufall, Appl. Phys. Lett. **81**, 2205 (2002).

[21] K. Lenz, H. Wende, W. Kuch, K. Baberschke, K. Nagy, and A. Jánossy, Phys. Rev. B **73**, 144424 (2006).

[22] M. Feygenson, X. Teng, S. E. Inderhees, Y. Yiu, W. Du, W. Han, J. Wen, Z. Xu, A. A. Podlesnyak, J. L. Niedziela, M. Hagen, Y. Qiu, C. M. Brown, L. Zhang, and M. C. Aronson, Phys. Rev. B **83**, 174414 (2011).

[23] E. Şaşıoğlu, C. Friedrich, and S. Blügel, Phys. Rev. B **87**, 020410 (2013).

[24] J. Callaway, A. K. Chatterjee, S. P. Singhal, and A. Ziegler, Phys. Rev. B **28**, 3818 (1983).

[25] J. A. Blackman, T. Morgan, and J. F. Cooke, Phys. Rev. Lett. **55**, 2814 (1985).

[26] S. Y. Savrasov, Phys. Rev. Lett. **81**, 2570 (1998).

[27] S. V. Halilov, A. Y. Perlov, P. M. Oppeneer, and H. Eschrig, Europhys. Lett. **39**, 91 (1997).

[28] A. Jacobsson, B. Sanyal, M. Ležaić, and S. Blügel, Phys. Rev. B **88**, 134427 (2013).

[29] P. Alippi, P. M. Marcus, and M. Scheffler, Phys. Rev. Lett. **78**, 3892 (1997).

[30] P. M. Marcus, F. Jona, and S. L. Qiu, Phys. Rev. B **66**, 064111 (2002).

[31] J. S. Faulkner, Prog. Mater. Sci. **27**, 1 (1982).

[32] O. K. Andersen, O. Jepsen, and G. Krier, *Lectures on Methods of Electronic Structure Calculations* (World Scientific, Singapore, 1994), p. 63.

[33] L. Vitos, Phys. Rev. B **64**, 014107 (2001).

[34] L. Vitos, H. L. Skriver, B. Johansson, and J. Kollár, Comp. Mat. Sci. **18**, 24 (2000).

[35] J. P. Perdew, K. Burke, and M. Ernzerhof, Phys. Rev. Lett. **77**, 3865 (1996).

[36] V. P. Antropov, M. I. Katsnelson, B. N. Harmon, M. van Schilfgaarde, and D. Kusnezov, Phys. Rev. B **54**, 1019 (1996).

[37] S. V. Halilov, H. Eschrig, A. Y. Perlov, and P. M. Oppeneer, Phys. Rev. B **58**, 293 (1998).

[38] M. Mašín, L. Bergqvist, J. Kudrnovský, M. Kotrla, and V. Drchal, Phys. Rev. B **87**, 075452 (2013).

[39] A. I. Liechtenstein, M. I. Katsnelson, V. P. Antropov, and V. A. Gubanov, J. Magn. Magn. Mater. **67**, 65 (1987).

[40] B. Skubic, J. Hellsvik, L. Nordström, and O. Eriksson, J. Phys.: Condens. Matter **20**, 315203 (2008).

[41] D. Landau and K. Binder, *Guide to Monte Carlo Simulations in Statistical Physics* (Cambridge University Press, Port Chester, NY, 2000).

[42] J. M. Karanikas, R. Sooryakumar, G. A. Prinz, and B. T. Jonker, J. Appl. Phys. **69**, 6120 (1991).

[43] M. O. C. Takahashi and H. Akai, J. Phys.: Condens. Matter **19**, 365233 (2007).

[44] E. Şaşıoğlu, L. M. Sandratskii, and P. Bruno, Phys. Rev. B **70**, 024427 (2004).

[45] I. Turek, J. Kudrnovský, V. Drchal, and P. Bruno, Philos. Mag. **86**, 1713 (2006).

[46] A. Jakobsson, E. Şaşıoğlu, P. Mavropoulos, M. Ležaić, B. Sanyal, G. Bihlmayer, and S. Blügel, Appl. Phys. Lett. **103**, 102404 (2013).

[47] L. Bergqvist, A. Taroni, A. Bergman, C. Etz, and O. Eriksson, Phys. Rev. B **87**, 144401 (2013).

[48] X. Tao, D. P. Landau, T. C. Schulthess, and G. M. Stocks, Phys. Rev. Lett. **95**, 087207 (2005).

[49] K. Chen and D. P. Landau, Phys. Rev. B **49**, 3266 (1994).

[50] A. Bergman, A. Taroni, L. Bergqvist, J. Hellsvik, B. Hjörvarsson, and O. Eriksson, Phys. Rev. B **81**, 144416 (2010).

[51] M. Pajda, J. Kudrnovský, I. Turek, V. Drchal, and P. Bruno, Phys. Rev. B **64**, 174402 (2001).

[52] X. Li, S. Schönecker, E. Simon, L. Bergqvist, H. Zhang, L. Szunyogh, J. Zhao, B. Johansson, and L. Vitos, Sci. Rep. **5**, 16654 (2015).

[53] C. Herring and C. Kittel, Phys. Rev. **81**, 869 (1951).

[54] B. Fultz, Phys. Rev. B **44**, 9805 (1991).